Journal of Chemical and Petroleum Engineering (JChPE)
Print ISSN: 2423-673X Online ISSN: 2423-6721

# Multi-Objective Optimization of Different Channel Shapes in Heat Exchangers

**Saeid Salimi, Reza Beigzadeh***

1. Department of Chemical Engineering, Faculty of Engineering, University of Kurdistan, Sanandaj, Iran
E-mail: saeidsalimi11@gmail.com
2. Department of Chemical Engineering, Faculty of Engineering, University of Kurdistan, Sanandaj, Iran
E-mail: r.beigzadeh@uok.ac.ir

**ARTICLE INFO**

**Article History**:
Received: 30 May 2021
Revised: 05 July 2021
Accepted: 21 July 2021

**Article type**: Research

**Keywords**:
Computational Fluid Dynamics (CFD),
Genetic Algorithm Multi-Objective Optimization,
Heat Exchanger,
Rectangular,
Serpentine,
Zigzag

**ABSTRACT**

The effect of geometric parameters of the zigzag, rectangular, and serpentine channels on convective heat transfer coefficient and pressure drop was investigated using computational fluid dynamics (CFD). The same boundary conditions were considered in all channels, and the number of steps was equal to 10. The simulations were performed for turbulent flows (liquid water as the operating fluid), and the Reynolds number (Re) range between 20000 and 60000 was selected. The zigzag channel showed the best thermal performance, and the serpentine channel showed the best hydraulic performance. The thermal-hydraulic performance (THP) factor was employed for comparing the channels. As the complexity of the channel's surfaces increased, the two parameters of convective heat transfer coefficient (positive factor) and pressure drop (negative factor) increased simultaneously. Therefore, predictive correlations for friction factor and Nusselt number were presented using a genetic algorithm (GA), The multi-objective optimization was performed to obtain the most appropriate Nusselt number and minimum friction factor as the two basic objective functions. The resulting Pareto set, which includes the optimum geometric dimensions of the heat exchangers, allows a designer to chooce the geometries based on higher heat transfer or lower pumping power.

## Introduction

Recently, a wide range of investigations have been conducted to enhance the efficiency of various heat exchangers to increase the heat transfer efficiency and decrease the fluid pumping costs[1]. Heat exchangers are significant equipment in factories [2]. There are some techniques to enhance the efficiency of heat exchangers. One of the most effective methods is employing optimal geometries of the channels that have the highest heat transfer and least pressure drop [3]. Studying fluid flow behavior in bends is very important to recognize and modify the performance and reduce energy loss[4]. There are some studies related to the turbulent flows at the channel bends by numerical, experimental, and theoretical procedures [5]. The flow of fluid through spiral, helical, or serpentine channels creates secondary flows that can increase the triple transfer phenomena in the curvatures [6].

* Corresponding Author: R.Beigzadeh (E-mail address: r.beigzadeh@uok.ac.ir)

*Journal of Chemical and Petroleum Engineering*, 2021, 55(2): 293-318.
*Publisher: University of Tehran, College of Engineering* *DOI: 10.22059/jchpe.2021.324733.1351*

The reduction of thermal boundary layer thickness is an important factor in decreasing thermal resistance and enhancing thermal efficiency in the zigzag channels [7]. Sharper bending angles increase the pressure drop because the flow turbulence is greater than circular bends. [8, 9].

Researchers have studied serpentine rectangular-bend channels. These studies included the effect of cross-sectional size and shape, inlet flow rate, number of pitches, changes in geometric parameters, size and geometric shape of the bend angles, and different boundary and initial conditions on thermal-hydraulic performance [10–15].

The serpentine channel geometries are specified by channel radius ($r$), bend curvature radius ($c$), and length of the straight sections ($l$). In the channels, the fluid flow through the curves creates a secondary flow that enhances heat and mass transfer. The secondary flow created by centrifugal forces in the curvature leads to eddy flows in the opposite direction of the flow and increases mass and heat transfer. The serpentine channels are used as the heat transfer, cooling, and mixing equipment in various parts of the industry, including solar thermal panels [4], medical, computer and electronic equipment, renewable energies, heat sinks, compact heat exchangers, and microreactors [16–20].

The techniques for increasing heat transfer are commonly used in the process and air conditioning equipment, thermal power plants, equipment, refrigerators, radiators, etc. In general, heat transfer enhancement techniques include three categories: 1. Active, 2. Passive, and 3. Combined methods [21]. The active methods deal with an external force to increase the heat transfer rate. For example, shocks from reciprocating pistons, using a magnetic field to bash small particles in a fluid flow, surface vibration and fluid vibration require an external actuator/power supply to begin performance improvement [22]. In the passive methods, there are no external force and the surface or geometric changes play a major role in this regard. Recently, wide researches have been conducted on the implementation of various types of passive methods in heat exchangers. In the passive method, additional components, rotary flow devices, modified surfaces, rough surfaces, stretched surfaces, and twisted and curved tubes can be used [23].

Imran et al. [24] performed a numerical and laboratory study of heat transfer in a spirally mini-channel coolant heat sink using various configuration models. The computational fluid dynamics model the single-phase convective heat transfer for the cooling water flow in the three-dimensional mini-channel with different geometries. Omidi et al. [25] investigated the effect of flow cross-section on the thermal and hydraulic performance of helical channels. According to the results, the spiral channel with the number of lobes equal to 6 had the highest $Nu$ and the lowest $f$. De la Torre et al. [26] studied the effect of four factors, including step length, zigzag angle, the radius of bend, and zigzag deformation in printed circuit heat exchangers. Then they presented correlations for $Nu$, and Fanning friction factor for $Re$ ranges less than 3200. According to the results, the effect of zigzag angle on thermal and hydraulic performance was more than other parameters. Donaldson et al. [27] investigated the hydraulic performance of serpentine mini-channels for the single-phase and two-phase fluid flow. They proposed a new correlation for the friction factor in non-turbulent fluid flows (laminar and transient flows). Korpys et al. [28] investigated the effect of the fluids with nanoparticles on the thermal performance in horizontal coils and turbulent flow. According to the results, the heat transfer in the CuO–water nanofluid in different volume fractions of nanoparticles was between 18 to 35% higher than pure water.

Changes in the geometry of the channels to increase the $Nu$ lead to an increase in $f$, which shows the need to optimize the geometric parameters. For this reason, multi-objective optimization is used by the genetic algorithm technique to find the optimal geometries of the channels. The heat exchanger designer can choose the optimal geometries based on his

preferences (more heat transfer or lower pumping cost). Beigzadeh et al. [29] performed a multi-objective optimization for corrugated channels with twisted tape. In the study, *f* and *Nu* were considered as the functions of the volume fraction of nanoparticles, twist ratios of twisted tape, and *Re*, and then the optimum variables were presented. Yang et al. [30] studied the multi-objective optimization of the printed circuit heat exchanger for improving temperature rise and reducing pressure drop. They obtained the optimal geometric dimensions of the investigated heat exchanger. Yildizeli et al. [31] investigated the multi-objective optimization of micro-channel heat sinks in the laminar flows. Two factors, including the *Nu* and the pumping power, were determined to evaluate the thermal-hydraulic performance of the heat exchanger. Geometric factors including channel height, width, and *Re* were considered as the design variables for the optimization.

In this study, the thermal-hydraulic performance (THP) of zigzag, rectangular and serpentine channels in the turbulent flow (Re=20000-60000) with water as working fluid was investigated using CFD. The geometric parameters of the channels were studied to determine the effects on the THP of the channels. In most same studies, the simultaneous effect of two geometric parameters on the thermal-hydraulic performance of the channels has not been investigated. The genetic algorithm technique was applied to present the accurate predictive formulas for *Nu* and *f* as functions of effective geometric parameters. Moreover, multi-objective optimization using GA was performed for each channel and Pareto sets of all optimum points for the channels were presented. The lack of a formula for predicting important thermal and hydraulic factors and optimal geometric points was noticeable. Changing the geometric dimensions to increase the heat transfer coefficient also leads to increasing the pressure drop. In this study, multi-objective optimization was used by the genetic algorithm technique to find the optimal geometries of the channels. Therefore, the heat exchanger designer has a wide range of optimal geometrical parameters to select the optimal geometries based on his preferences (more heat transfer or lower pumping cost).

## Computational model

The first step after sufficient knowledge of the problem is to design the desired geometry. The purpose of this study is to investigate the effect of geometric parameters of heat exchanger channels in turbulent flows and, in the next step, developing predictive correlations and multi-objective optimization for this type of channel. The three-dimensional geometry of each channel must be drawn with specific geometric parameters.

### Design and geometric characteristics of the channels

Fig. 1 shows the geometric parameters of the zigzag channel. The hydraulic diameter of the channel was equal to 0.01 m and the number of steps of the channel was 10. The same length of the inlet and outlet of the channel was determined equal to 0.15 m. In the zigzag channels, $L_s$ is the straight parts of the channel and Θ is the bend angles. According to Eq. 1, the length of the zigzag channel flow path will be obtained:

$$L_{Path} = L_{in} + L_{out} + \sum_{i=1}^{20} L_{S_i} \quad (1)$$

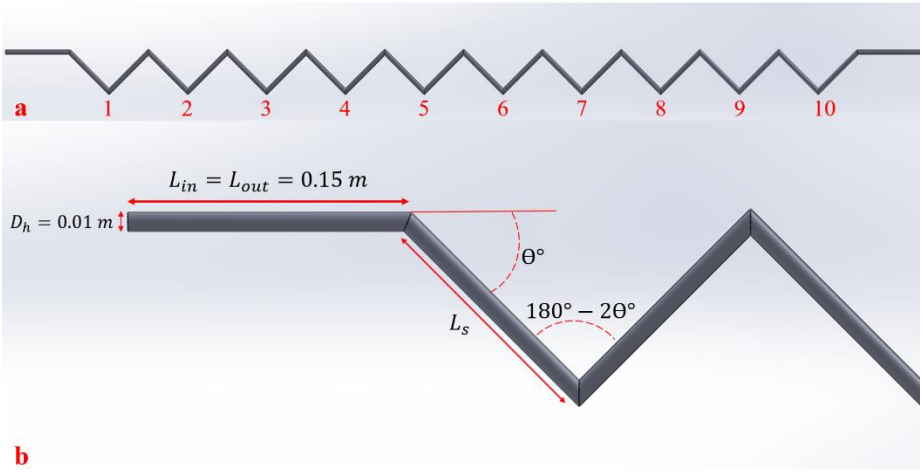


**Fig. 1**. (a) General view and the number of steps of the zigzag channel and (b) Geometric characteristics of the zigzag channel

Fig. 2 shows the geometric parameters of the rectangular channel. The diameter of the channel was determined to be 0.01 m and the number of steps of the channel was 10. Similar to the zigzag channel, the input and output lengths were considered to be 0.15 m. Ls are the straight section adjacent to the bends in the zigzag channels and α is the bend angles. The length of the flow path in the rectangular channel is obtained by Eq. 2:

$$L_{Path} = L_{in} + L_{out} + \sum_{i=1}^{19} X_i + \sum_{i=1}^{20} L_{S_i} + \sum_{i=1}^{40} L_{Cr_i} \tag{2}$$

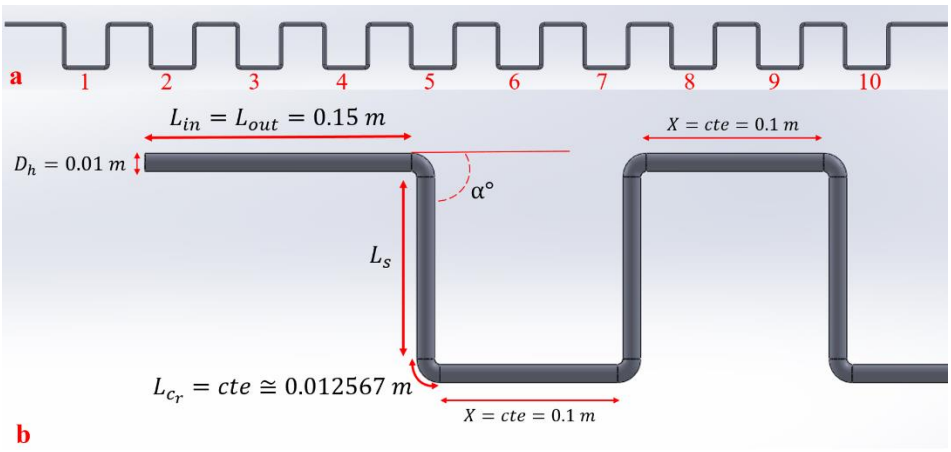


**Fig. 2**. (a) General view and the number of steps of the rectangular channel and (b) Geometric characteristics of the rectangular channel

Fig. 3 shows the geometric parameters of the serpentine channel. Like the previous two channels, ten steps and a length of 0.15 m were determined for the input and output of the channel. The total channel length for the serpentine channel is obtained as follows:

$$L_{Path} = L_{in} + L_{out} + \sum_{i=1}^{20} L_{S_i} + \sum_{i=1}^{20} L_{C_i} \tag{3}$$

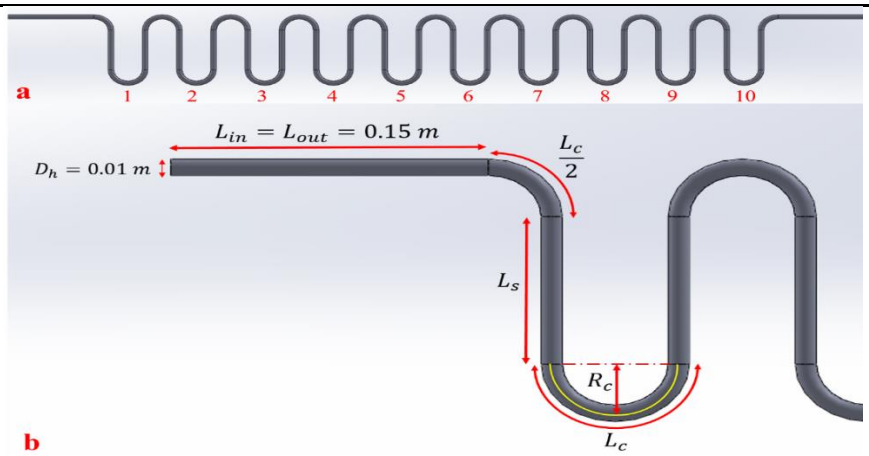


**Fig. 3**. (a) General view and the number of steps of the serpentine channel and (b) Geometric characteristics of the serpentine channel

Table 1 reports the geometric characteristics of zigzag channels. A total of 27 models were designed for investigating the zigzag channel. Bend angles between 5 and 45 degrees were considered, and the length of the straight part from 0.13 to 0.19 m was selected as a variable. Table 2 reports the geometric characteristics of the rectangular channels. The bend angles between 10 and 90 degrees were applied for the channels. Table 3 shows the geometric characteristics of the serpentine channels. The length of each part of the channels and their flow path are listed in the tables.

**Table 1**. Geometrical parameters of the zigzag channels.

| Case number | $L_s$ (m) | Θ (°) | $L_{path}$ (m) |
|---|---|---|---|
| **1** | 0.13 | 5 | 2.9 |
| **2** | | 10 | |
| **3** | | 15 | |
| **4** | | 20 | |
| **5** | | 25 | |
| **6** | | 30 | |
| **7** | | 35 | |
| **8** | | 40 | |
| **9** | | 45 | |
| **10** | 0.16 | 5 | 3.5 |
| **11** | | 10 | |
| **12** | | 15 | |
| **13** | | 20 | |
| **14** | | 25 | |
| **15** | | 30 | |
| **16** | | 35 | |
| **17** | | 40 | |
| **18** | | 45 | |
| **19** | 0.19 | 5 | 4.1 |
| **20** | | 10 | |
| **21** | | 15 | |
| **22** | | 20 | |
| **23** | | 25 | |
| **24** | | 30 | |
| **25** | | 35 | |
| **26** | | 40 | |
| **27** | | 45 | |

**Table 2**. Geometrical parameters of the rectangular channels.

| Case number | $L_s$ (m) | α (°) | $L_{cr}$ (m) | $L_{path}$ (m) |
|---|---|---|---|---|
| **1** | 0.07 | 10 | 0.0125 | 4.102 |
| **2** | | 20 | | |
| **3** | | 30 | | |
| **4** | | 40 | | |
| **5** | | 50 | | |
| **6** | | 60 | | |
| **7** | | 70 | | |
| **8** | | 80 | | |
| **9** | | 90 | | |
| **10** | 0.1 | 10 | 0.0125 | 4.702 |
| **11** | | 20 | | |
| **12** | | 30 | | |
| **13** | | 40 | | |
| **14** | | 50 | | |
| **15** | | 60 | | |
| **16** | | 70 | | |
| **17** | | 80 | | |
| **18** | | 90 | | |
| **19** | 0.13 | 10 | 0.0125 | 5.302 |
| **20** | | 20 | | |
| **21** | | 30 | | |
| **22** | | 40 | | |
| **23** | | 50 | | |
| **24** | | 60 | | |
| **25** | | 70 | | |
| **26** | | 80 | | |
| **27** | | 90 | | |

**Table 3**. Geometrical parameters of the serpentine channels.

| Case number | $L_s$ (m) | $R_c$ (m) | $L_c$ (m) | $L_{path}$ (m) |
|---|---|---|---|---|
| **1** | 0.09 | 0.02 | 0.0628 | 3.356 |
| **2** | | 0.03 | 0.0942 | 3.984 |
| **3** | | 0.04 | 0.1256 | 4.613 |
| **4** | 0.12 | 0.02 | 0.0628 | 3.956 |
| **5** | | 0.03 | 0.0942 | 4.584 |
| **6** | | 0.04 | 0.1256 | 5.213 |
| **7** | 0.15 | 0.02 | 0.0628 | 4.556 |
| **8** | | 0.03 | 0.0942 | 5.184 |
| **9** | | 0.04 | 0.1256 | 5.813 |

A regular and organized hexahedral mesh was used for meshing the model domains. The boundary layer mesh was used to meshing the areas close to the wall, as shown in Fig. 4. The

channel input and output area were set as the velocity inlet and pressure outlet boundary conditions.

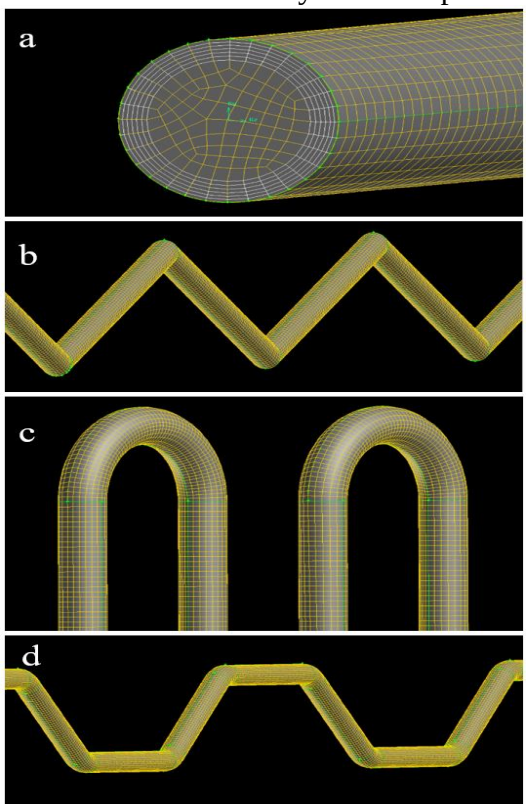


**Fig.4**. (a) The boundary layer mesh for all channels and meshed (b) zigzag, (c) serpentine, and (d) rectangular channels

## CFD Modeling

Computational fluid dynamics is a science that can study fluid flow, heat transfer, chemical reactions, etc. by solving mathematical equations using numerical analysis. It is useful in designing heat exchanger systems in troubleshooting / optimizing by proposing design modifications.

The purpose of this study is to investigate the effect of geometric parameters of channels on thermal-hydraulic performance, so special formulas are needed to obtain the results. The different sections are explained below:

The governing equations used for the study include the equations of continuity, momentum, and energy as follows:

$$\frac{\partial}{\partial x_i}(\rho . u_i) = 0 \tag{4}$$

$$\frac{\partial}{\partial x_i}\left(\rho . u_i . u_j\right) = -\frac{\partial P}{\partial x_i} + \frac{\partial}{\partial x_j}\left[(\mu + \mu_t)\frac{\partial u_i}{\partial x_j}\right] \tag{5}$$

$$\frac{\partial}{\partial x_i}\left(u_i(\rho . E + P)\right) = \frac{\partial}{\partial x_i}(k_{eff}\frac{\partial T}{\partial x_i} + u_i \tau_{ij}) \tag{6}$$

Eq. 4 is the continuity equation, in which $\rho$ is the density and $u_i$ is the velocity vector. Eq. 5 is the momentum equation, in which $P$ is the pressure, $\mu$ and $\mu_t$ are the molecular and turbulent flow viscosity, respectively. Eq. 6 is the energy equation, in which $k_{eff}$ is the effective thermal conductivity is obtained by the formula $k_{eff} = k + k_t$ in which $k_t$ is the turbulent thermal conductivity. Also, $\tau_{ij}$ represents the stress vector. The formula for calculating the logarithmic temperature difference is as follows:

$$\Delta T_{LMTD} = \frac{(T_w - T_{in}) - (T_w - T_{out})}{Ln(\frac{T_w - T_{in}}{T_w - T_{out}})} \quad (7)$$

The heat transfer rate was obtained as follows:

$$\dot{Q} = \dot{m}.C_P.(T_{out} - T_{in}) \quad (8)$$

The heat transfer coefficient is obtained from the following formula:

$$h = \frac{\dot{Q}}{A.\Delta T_{LMTD}} \quad (9)$$

The formula for calculating the Reynolds number is as follows:

$$Re = \frac{\rho.u.D_h}{\mu} \quad (10)$$

Using the obtained parameters, the friction factor formula will be as follows:

$$f = \frac{2.\Delta P.D_h}{\rho.u^2.L_{Path}} \quad (11)$$

The Nusselt number is obtained using the following formula:

$$Nu = \frac{h.D_h}{k} \quad (12)$$

Finally, to calculate the thermal-hydraulic performance factor [32,33]:

$$THP = \frac{(Nu/Nu_S)}{(f/f_S)^{1/3}} \quad (13)$$

where, *S* refers to the straight channel. The model of two standard equations k-ε, which is an acceptable model for the turbulent flows, has been used in the study and its validity and accuracy have been examined in the following sections. The formulas used in the two equations (transfer equations) are obtained as follows.

The following equation for calculating kinetic energy:

$$\frac{\partial}{\partial t}(\rho.k) + \frac{\partial}{\partial x_i}(\rho.k.u_i) = \frac{\partial}{\partial x_j}\left[(\mu + \frac{\mu_t}{\sigma_k})\frac{\sigma_k}{\partial x_j}\right] + P_k + \rho.\varepsilon \quad (14)$$

To calculate energy dissipation:

$$\frac{\partial}{\partial t}(\rho.\varepsilon) + \frac{\partial}{\partial x_i}(\rho.\varepsilon.u_i) = \frac{\partial}{\partial x_j}\left[(\mu + \frac{\mu_t}{\sigma_\varepsilon})\frac{\sigma_\varepsilon}{\partial x_j}\right] + C_{1\varepsilon}\frac{\varepsilon}{k}P_k - C_{2\varepsilon}\rho\frac{\varepsilon^2}{k} \quad (15)$$

There are the following parameters, and Table 4 reports the used constants:

$$\mu_t = \mu.C_\mu\frac{k^2}{\varepsilon} \quad (16)$$

$$P_k = -\rho\overline{u_i'u_j'}\frac{\partial u_i}{\partial x_j} \quad (17)$$

**Table 4**. Constants used in the standard k-ε model

| $C_{1\varepsilon}$ | $C_{2\varepsilon}$ | $C_{\mu}$ | $\sigma_k$ | $\sigma_\varepsilon$ |
|---|---|---|---|---|
| **1.44** | 1.92 | 0.09 | 1 | 1.3 |

The pressure-based solver was selected and the minimum accuracy for convergence of $10^{-6}$ was considered. All the thermo-physical properties of the fluid, which is liquid water in the present study, have been calculated at the mean temperature of the fluid inlet and outlet. The SIMPLE algorithm was used to solve and couple the pressure-velocity equations simultaneously. Then, the second-order solution method was used for momentum and energy equations and the first-order solution was employed for turbulent kinetic energy equations and energy dissipation.

The model validation was performed using the empirical correlations. Eq. 18 was proposed by Taler et al. [34] for obtaining *Nu* for turbulent flows in a straight channel. The comparison between correlation and simulation results is reported in Fig. 5, which shows the acceptable errors.

$$Nu = 0.00881 Re^{0.8991} Pr^{0.3911}$$
$$Valid\ for: 3 \times 10^3 \le Re \le 10^6 \quad ; \quad 3 < Pr \le 1000 \tag{18}$$

In addition, validation for the friction factor in straight channels was performed according to the Blasius formula [35] and the high accuracy was obtained. The results can be seen in Fig. 6.

$$f = \frac{0.316}{Re^{1/4}} \tag{19}$$

The mesh independence procedure was performed for the pressure drop changes and is shown in Fig. 7. For the number of approximately 410000 meshes, the changes of less than 5 Pascal (less than 1%) were observed. The result of this test was used for the simulated channels.

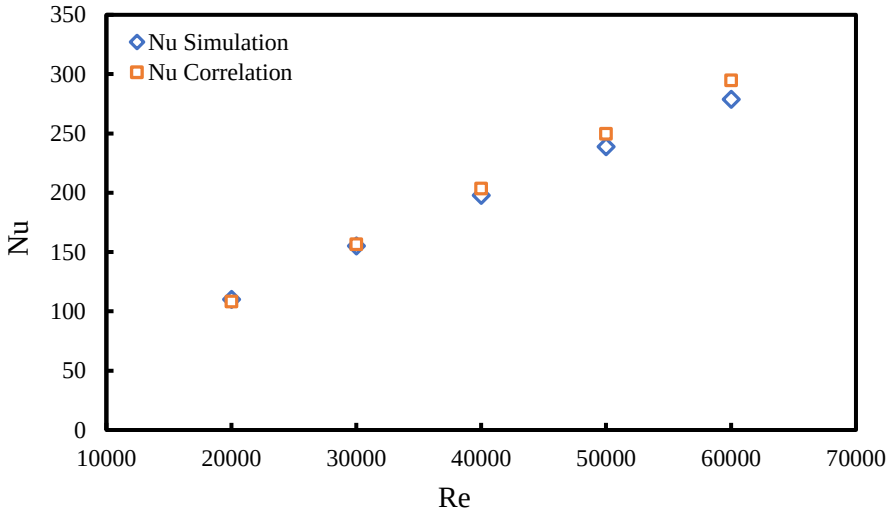


**Fig. 5**. Validation for Nusselt number in the straight channel

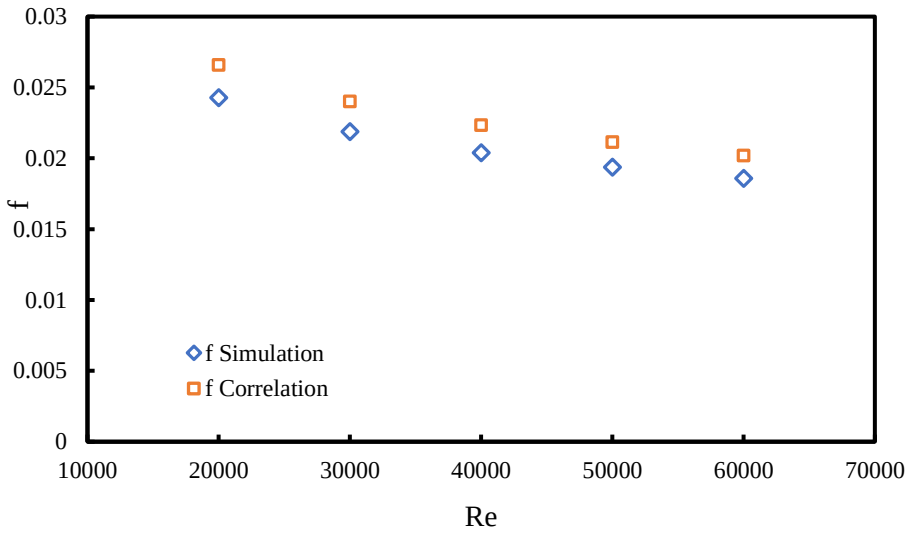


**Fig. 6**. Validation for friction factor in the straight channel

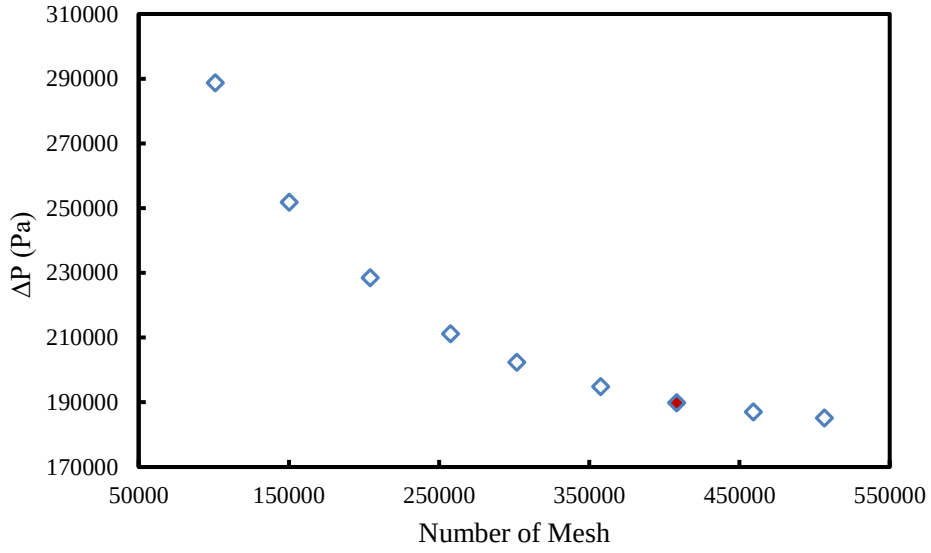


**Fig. 7**. Mesh independence test

## Genetic Algorithm Modeling

Genetic algorithm (GA) is an important search and optimization technique that has become very popular in engineering optimization problems. The GA was inspired by the principles of genetics and Darwin's theory of biological evolution. The optimization method starts with the initial set of random solutions (population) and evolves through better repetitions (generations) towards better solutions. The main components of GA include competency assessment, parental selection, elitism, combination, and mutation operators. The steps for the GA method are generally as follows:

1. Stage 1: Generate the initial population by random chromosomes of constant initial size (each individual in the population is an appropriate solution to the problem and is defined by optimization variables).
2. Stage 2: Assess the suitability (value of the objective function) of the solutions (chromosomes) in the population

3. Stage 3: produce a new population with the following steps:
   - Selection: Selection of two solutions (parents) based on merit values for a combination.
   - Elitism: Copying the best chromosome or some of the best chromosomes to a new population.
   - Combination: The creation of two new chromosomes (children) through the combination of two parents.
   - Mutation: Random changes in offspring chromosomes.
   - Replacement: Replacing old chromosomes with new ones and producing a new generation.
4. Stage 4: Eventually, the operation will stop if a suitable answer is found. Otherwise, it will return to the second step.

The genetic algorithm mimics the evolutionary process of nature to find an optimal solution. Optimization algorithms can be divided into two categories. The first category, known as single-objective optimization, involves finding the overall minimum or maximum of an aggregate function, which typically consists of a set of individual goals. The second category is multi-objective optimization, which involves the simultaneous optimization of several, often conflicting, goals. In multi-objective optimization, a set of optimal non-dominant solutions is produced, which is called the Pareto domain.

For the investigated zigzag channels, a relationship between Nusselt number and Reynolds number, and the ratio of bend angle and the length of the straight part of the channel to the hydraulic diameter were considered. The same was done for the friction factor. The correlations presented for *Nu* and *f* are as follows:

$$Nu = C_1 Re^{C_2} \left(\frac{\theta}{\pi}\right)^{C_3} \left(\frac{L_S}{D_h}\right)^{C_4} \tag{20}$$

$$f = C_1 Re^{C_2} \left(\frac{\theta}{\pi}\right)^{C_3} \left(\frac{L_S}{D_h}\right)^{C_4} \tag{21}$$

where $C_i$ is the constant of the equations.

In the rectangular channel, the relationship between the *Nu* and the *Re*, as well as the ratio of the bend angle and the length of the straight part of the channel to the part with the fixed horizontal length, were considered. The same was done for the friction factor. The correlations presented for the *Nu* and the *f* are as follows:

$$Nu = C_1 Re^{C_2} \left(\frac{\alpha}{\pi}\right)^{C_3} \left(\frac{L_S}{X}\right)^{C_4} \tag{22}$$

$$f = C_1 Re^{C_2} \left(\frac{\alpha}{\pi}\right)^{C_3} \left(\frac{L_S}{X}\right)^{C_4} \tag{23}$$

Finally, for the serpentine channel, the relationship between the *Nu* and the *Re*, as well as the ratio of the bend radius to the hydraulic diameter and the length of the straight part of the channel to the hydraulic diameter were considered. The correlations presented for the *Nu* and the *f* are as follows:

$$Nu = C_1 Re^{C_2} \left(\frac{L_S}{D_h}\right)^{C_3} \left(\frac{R_C}{D_h}\right)^{C_4} \tag{24}$$

$$f = C_1 Re^{C_2} \left(\frac{L_S}{D_h}\right)^{C_3} \left(\frac{R_C}{D_h}\right)^{C_4} \tag{25}$$

The considered objective (error) functions between the target and predicted data for *Nu* and *f* are as follows:

$$E_{Nu}(C_1, C_2, C_3, C_4) = \frac{1}{n}\sum_{i=1}^{N}(Nu_i^{Target} - Nu_i^{Pred})^2 \quad (26)$$

$$E_f(C_1, C_2, C_3, C_4) = \frac{1}{n}\sum_{i=1}^{N}(f_i^{Target} - f_i^{Pred})^2 \quad (27)$$

in which n is the number of data. The target data are CFD output and Pred is related to the predicted data.

The genetic algorithm technique can obtain optimal values of the correlation constants using a random numerical search method. The advantage of using the genetic algorithm technique over the classical methods, such as the least squares method, is obtaining the general optimum answer.

In addition, multi-objective GA is used to achieve optimal geometric parameters in all three types of channels, which leads to the minimum pressure drop and maximum heat transfer. Therefore, we select two objective functions for each channel separately to minimize the friction factor (*f*) and maximize the Nusselt number (*Nu*).

Objective functions for the zigzag channels are defined as follows:

$$OF_1\left(\left(\frac{\theta}{\pi}\right), \left(\frac{L_S}{D_h}\right), Re\right) = \frac{1}{Nu} \quad (28)$$

$$OF_2\left(\left(\frac{\theta}{\pi}\right), \left(\frac{L_S}{D_h}\right), Re\right) = f \quad (29)$$

And for the rectangular channels:

$$OF_1\left(\left(\frac{\alpha}{\pi}\right), \left(\frac{L_S}{X}\right), Re\right) = \frac{1}{Nu} \quad (30)$$

$$OF_2\left(\left(\frac{\alpha}{\pi}\right), \left(\frac{L_S}{X}\right), Re\right) = f \quad (31)$$

Finally, for the serpentine channels, the objective functions were as follows:

$$OF_1\left(\left(\frac{L_S}{D_h}\right), \left(\frac{R_C}{D_h}\right), Re\right) = \frac{1}{Nu} \quad (32)$$

$$OF_2\left(\left(\frac{L_S}{D_h}\right), \left(\frac{R_C}{D_h}\right), Re\right) = f \quad (33)$$

In the GA modeling procedure, the number of the chromosome for the initial population and the crossover fraction were 100 and 0.8, respectively. The number of elite children (chromosomes with the greatest fitness in each generation) was chosen to be 2. GA search was discontinued after 200 generations in which it was reached the optimal results.

## Results and discussion

The simulation results for the zigzag, rectangular and serpentine channels were presented, and then the optimization outputs by the genetic algorithm method for all channels were presented.

### Simulation by Computational Fluid Dynamics Method

Fig. 8 illustrates the turbulent intensity distribution for the zigzag channel in the Re=60000. Increasing the bend angle leads to an increase in the turbulence intensity. The maximum occurs exactly in the areas after each bend due to the more velocity gradients in that area.

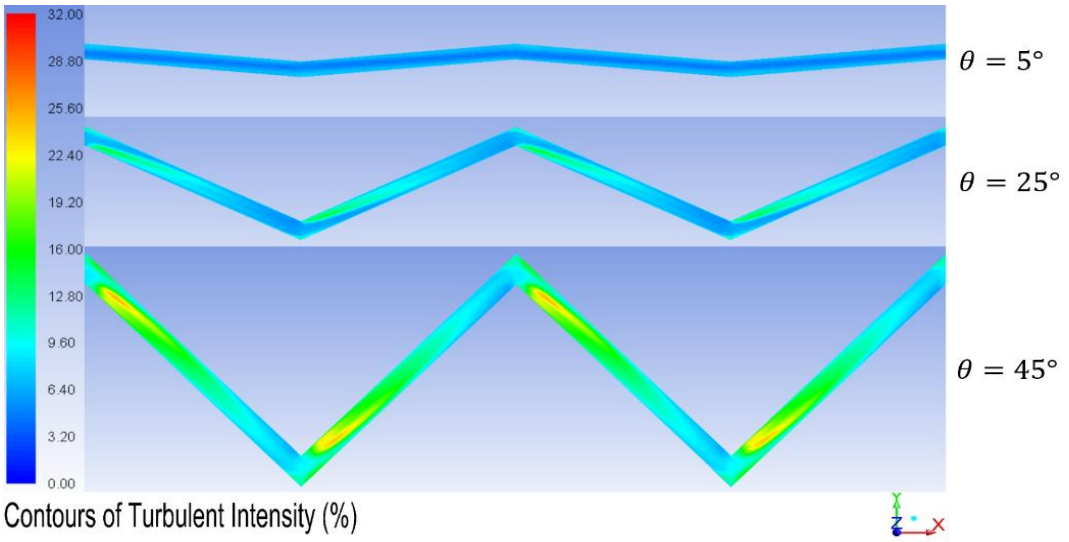


**Fig. 8**. Turbulent intensity distribution for the zigzag channel at Re = 60000 for bend angles of 5, 25, and 45°

The thermal-hydraulic performance factor (Eq. 13) was investigated due to the simultaneous effect of the channel geometries on the heat transfer coefficient and pressure drop. Fig. 9 shows the thermal-hydraulic performance (THP) values for the investigated zigzag channels. With increasing the bend angle, the thermal-hydraulic performance of the channels is reduced. This shows that the effect of increasing the bend angle on pressure drop was greater than the effect of the convective heat transfer coefficient. Increasing the fluid velocity also reduces the thermal-hydraulic performance of the zigzag channels. The effect of increasing the length of the straight part of the channels in the study area was much less.

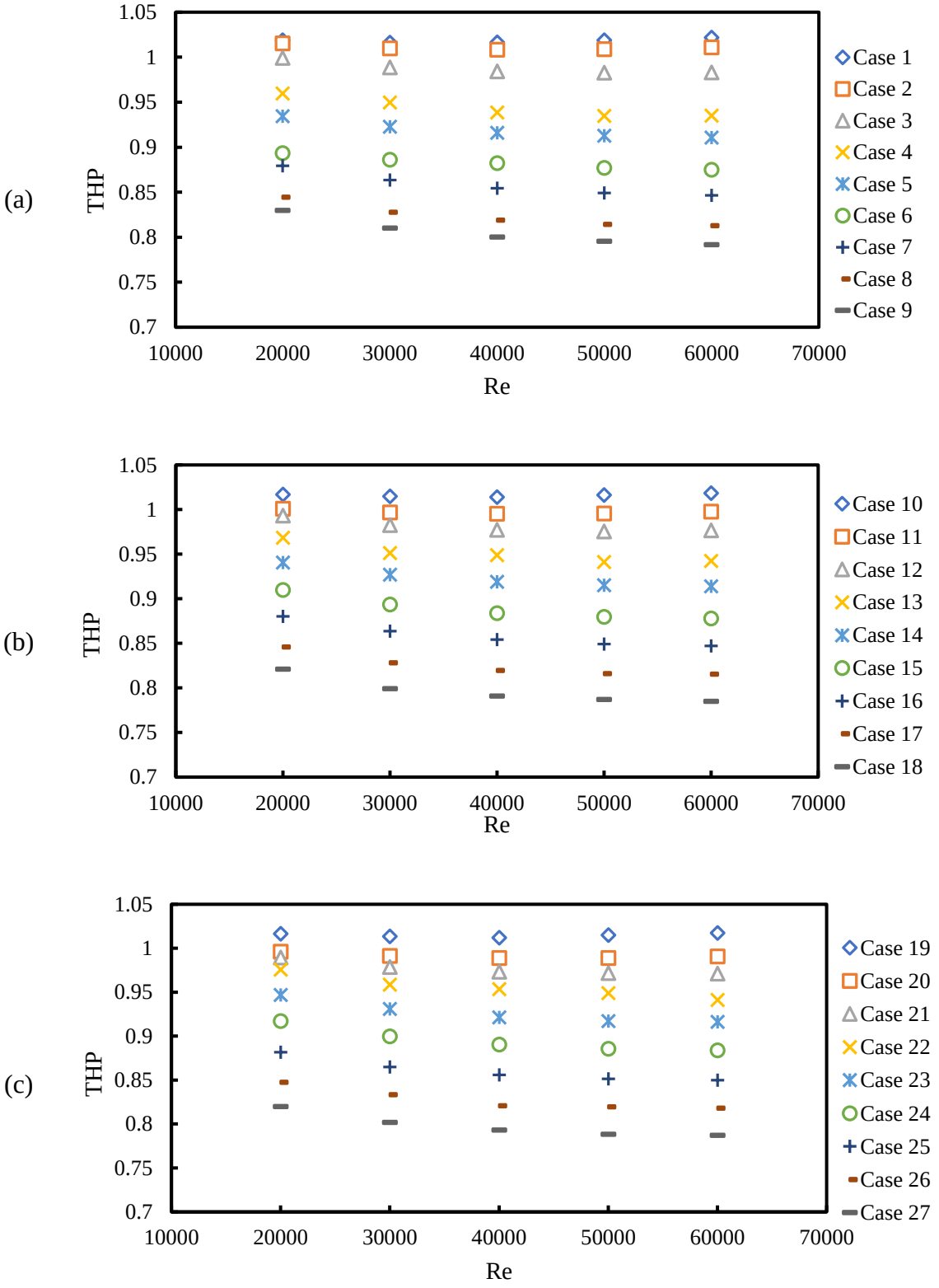


**Fig. 9**. Thermal-hydraulic performance diagrams for the zigzag channels with the length of the straight section: (a) 13 cm (b) 16 cm and (c) 19 cm

Fig. 10 shows the turbulent intensity distribution for the rectangular channels in the Re=60000 at bend angles of 10, 50, and 90°. Increasing the bend angle increases the intensity of the turbulence, especially in the parts after each bend. According to the modeling results, the

level of turbulence intensity in the rectangular channel was lower than the zigzag channel. The behavior of the fluid after passing through the bends plays a very important role in determining the thermal and hydraulic performance.

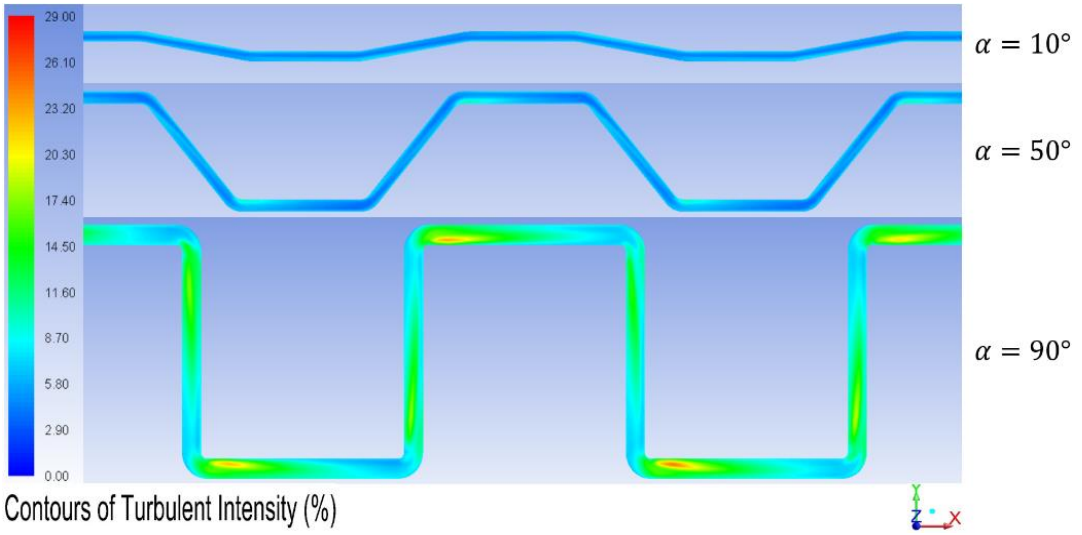


**Fig. 10**: Turbulent intensity distribution for rectangular channel at Re = 60000 for bend angles of 10, 50, and 90°

Fig. 11 shows the thermal-hydraulic performance of the rectangular channels for Re=20000-60000. The effect of increasing the bend angle on THP is greater than other parameters. With increasing bend angles from 40 to 90°, the THP of the channels decreases. However, for bend angles from 10 to 30°, different functional behavior was observed in different *Re*.

Fig. 12 shows the turbulent intensity distribution for the serpentine channels. According to the figure, the level of turbulent intensity in the serpentine channel is much lower than in the zigzag and rectangular channels.

Fig. 13 shows the thermal-hydraulic performance of the serpentine channels. In all channels, with increasing the radius of the curve, the thermal-hydraulic performance is increased. This indicates that the negative effect of increasing the pressure drop at smaller curvatures was greater than the positive effect of increasing the heat transfer coefficient.

(a)

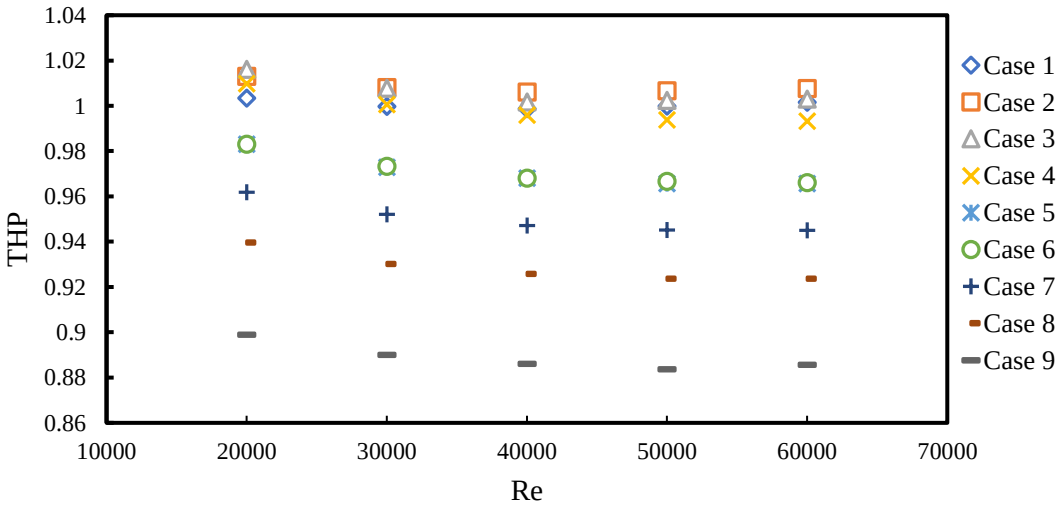

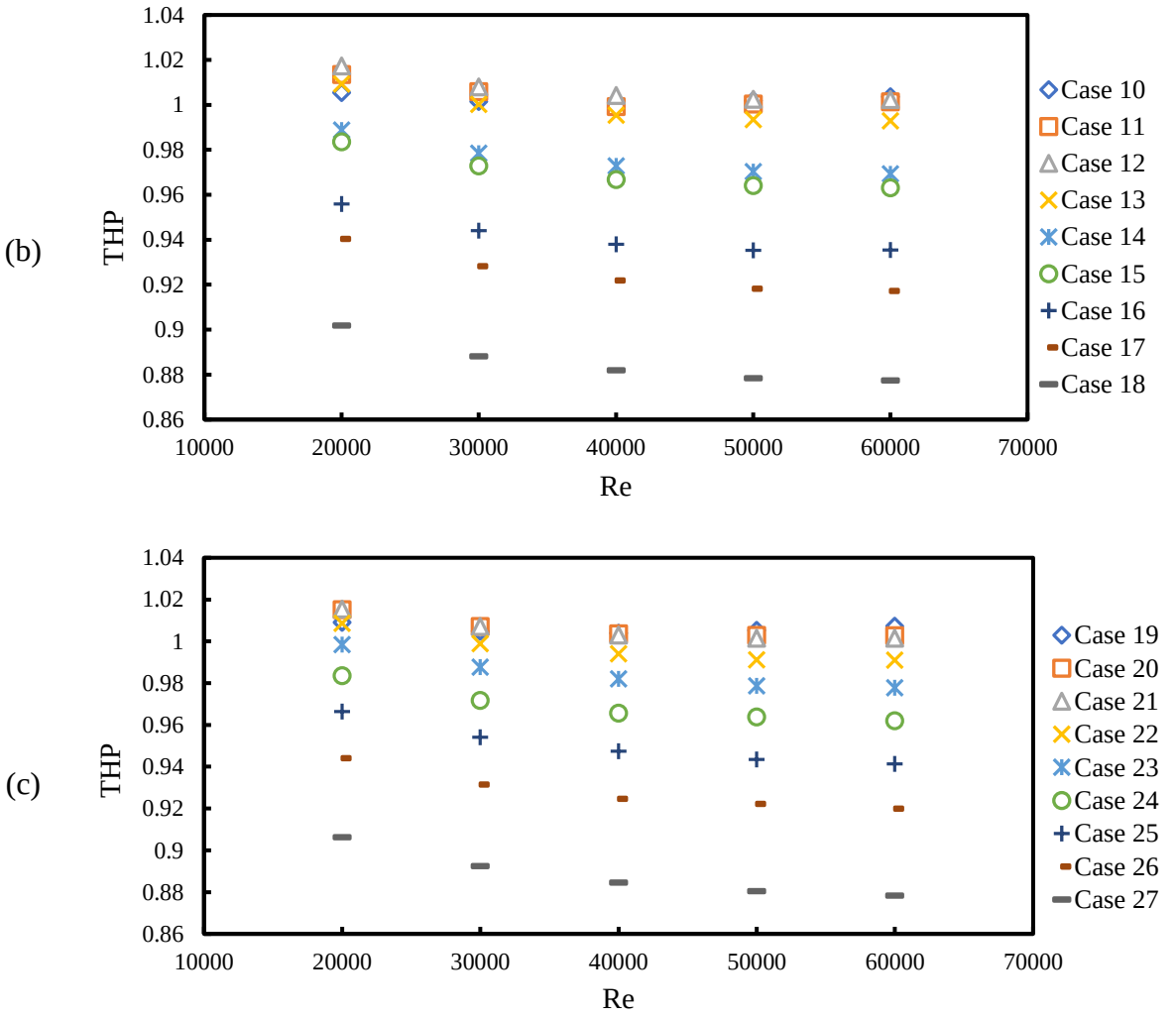


**Fig. 11**. Thermal-hydraulic performance for the rectangular channels with the length of the straight section: (a) 7 cm (b) 10 cm, and (c) 13 cm

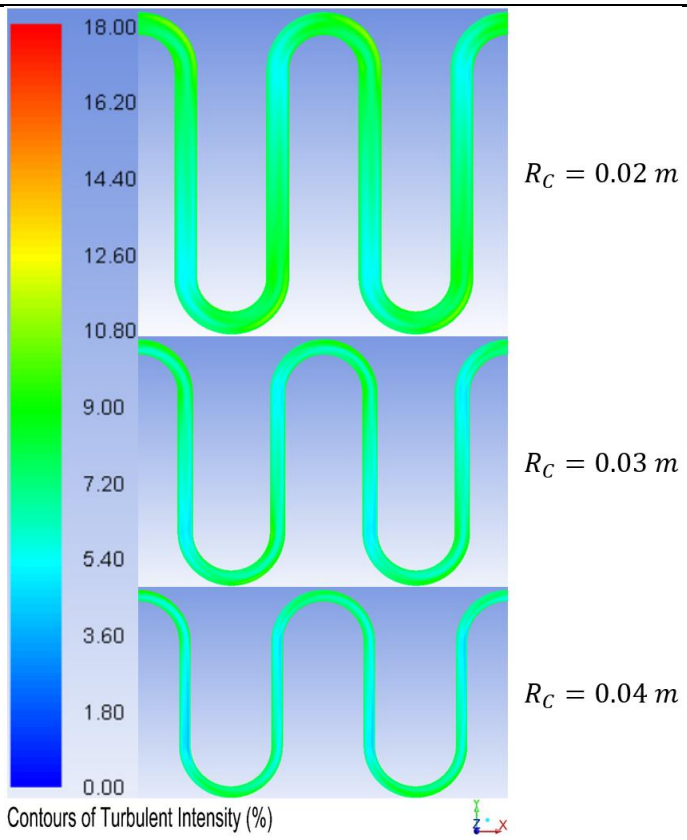


**Fig. 12**. Turbulent intensity distribution for the serpentine channels at Re=60000 for the radius of curvatures of 2, 3, and 4 cm

(a)

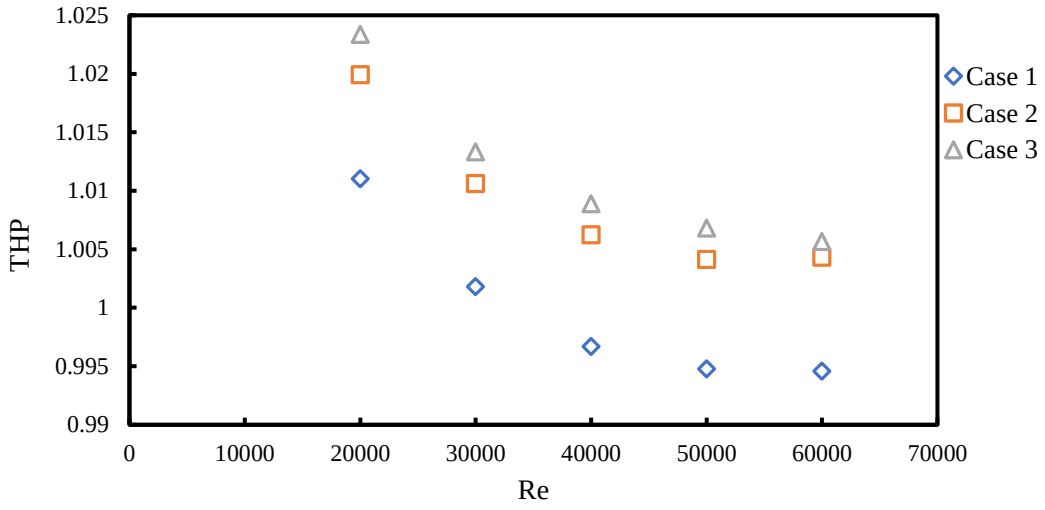

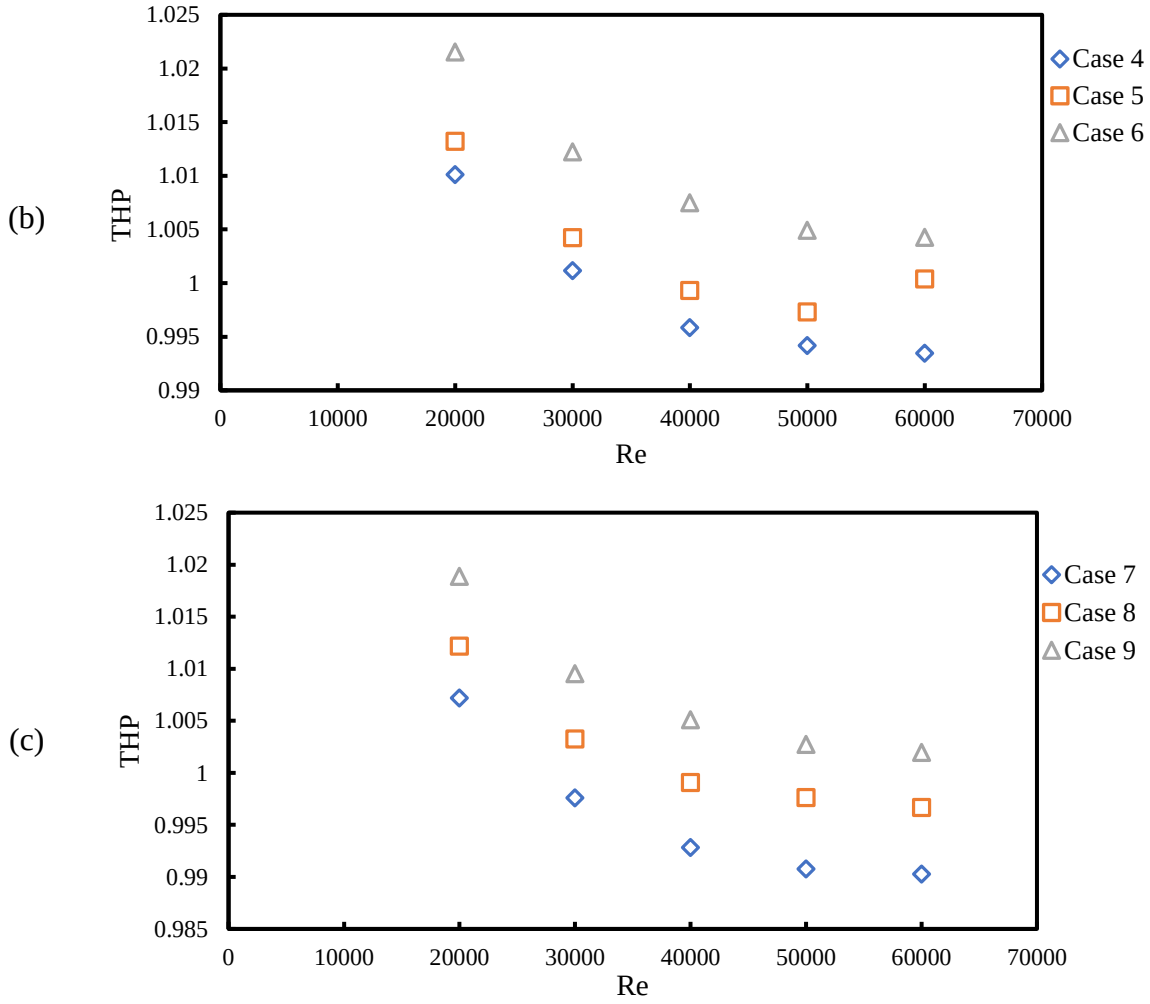


**Fig. 13**. Thermal-hydraulic performance for the serpentine channels with the straight section length: (a) 9 cm (b) 12 cm and (c) 15 cm

More heat transfer coefficients were obtained for the zigzag channels. In addition, the best thermal performance was for the channel with a bend angle of 45°, *Ls* = 0.13 m, and *Re* = 60000 in the investigated zigzag channels. The Nu in this channel was 41% higher than the straight channel. Also, the higher pressure drop was for the zigzag channels. The f in a zigzag channel with the bend angle of 45°, *Ls* = 0.13 m, and *Re* = 60000 was increased by 465% compared to the straight channel. Eventually, the best THP was obtained for the serpentine channel with *Rc* = 0.04 m, *Ls* = 0.09 m, and Re = 20000. Moreover, the weakest THP was for the zigzag channel with a bend angle of 45° and *Ls* = 0.13 m and *Re* = 60000. Therefore, the zigzag channels require the most pumping cost.

## Optimization by Genetic Algorithm

In this section, the correlations for predicting the Nusselt number and friction factor and the results of multi-objective optimization by genetic algorithm (GA) for each type of the investigated channels, are presented. The multi-objective optimization by GA approach was used to applied optimal geometries, which cause maximum possible heat transfer rate and minimum pressure drop. The optimal solutions lead to a trade-off between *Nu* and *f*.

*Zigzag channels*

The optimum constants of the Eqs. 20 and 21 were obtained using the GA method. It was observed that the prediction accuracy was low for the bend angles of 5 and 10° due to large friction factor changes in these two angles. Therefore, the correlation constants were optimized for 15°≤Θ≤ 45°. The resulting relations for Nusselt number and friction factor were obtained as follows:

$$Nu = 0.047Re^{0.856}\left(\frac{\theta}{\pi}\right)^{0.141}\left(\frac{L_S}{D_h}\right)^{-0.1} \quad (34)$$

$$f = 3.882Re^{-0.134}\left(\frac{\theta}{\pi}\right)^{0.946}\left(\frac{L_S}{D_h}\right)^{-0.404} \quad (35)$$

*Valid for* $15° \le \Theta \le 45°$

The mean relative errors (MREs) for predicted *Nu* and *f* in zigzag channels were 2.58% and 7.61%, respectively.

Fig. 14 shows the Pareto curve for the zigzag channels. This curve shows all the optimal points obtained from optimizing the two objective functions $OF_1$ and $OF_2$ (Eqs. 28 and 29). According to the figure, there is an inverse relationship between the two objective functions.

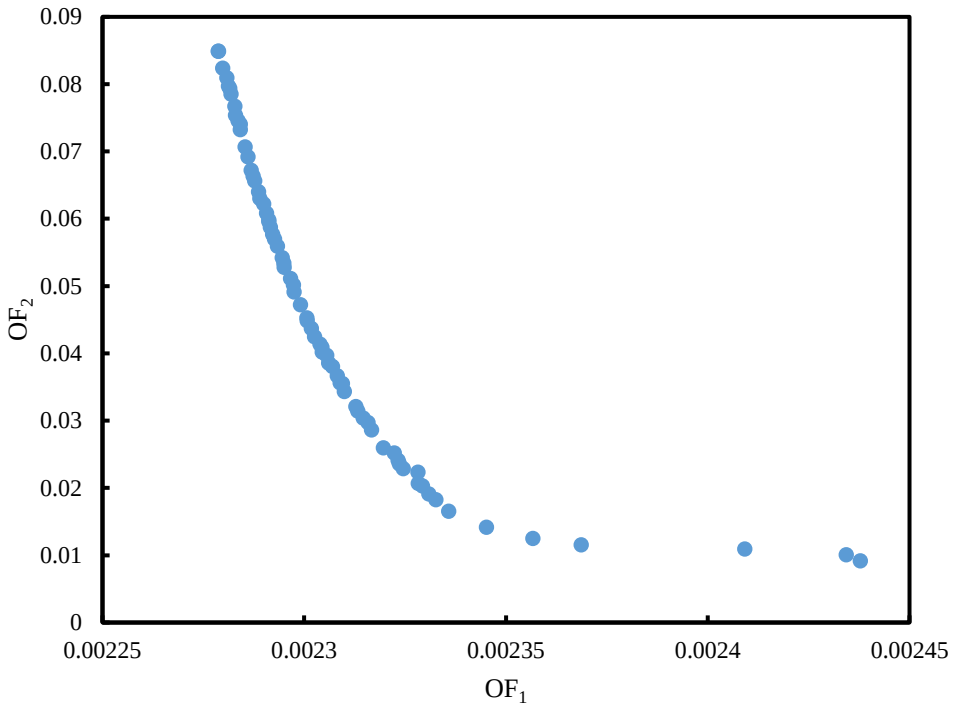


**Fig. 14**. Pareto optimal points for the zigzag channel

Some optimal points based on geometric parameters in different *Re* are reported in Table 5. It is clear that the effect of *Re* was significant, and the higher *Nu* and lower *f* were obtained at higher *Re*.

**Table 5**. Some of the optimal points selected for the zigzag channels.

| Re | Θ/ π | $L_s/D_h$ | Nu | f |
|---|---|---|---|---|
| 20000 | 0.030 | 18.94 | 160.15 | 0.01129 |

| | | | | |
|---|---|---|---|---|
| 20000 | 0.145 | 13.06 | 169.96 | 0.05856 |
| 20000 | 0.250 | 13.00 | 171.35 | 0.09843 |
| 20000 | 0.040 | 14.50 | 165.18 | 0.01669 |
| 20000 | 0.074 | 13.29 | 168.06 | 0.03066 |
| 20000 | 0.053 | 14.07 | 166.31 | 0.02184 |
| 20000 | 0.209 | 13.01 | 170.91 | 0.08301 |
| 30000 | 0.028 | 18.56 | 226.88 | 0.01023 |
| 30000 | 0.250 | 13.02 | 242.42 | 0.09315 |
| 30000 | 0.037 | 13.95 | 234.33 | 0.01476 |
| 30000 | 0.046 | 13.44 | 235.95 | 0.01854 |
| 30000 | 0.130 | 13.13 | 239.98 | 0.04994 |
| 30000 | 0.091 | 13.72 | 237.72 | 0.03489 |
| 30000 | 0.062 | 13.56 | 236.72 | 0.02439 |
| 40000 | 0.028 | 19.00 | 289.51 | 0.00964 |
| 40000 | 0.161 | 13.08 | 308.03 | 0.05886 |
| 40000 | 0.052 | 13.18 | 302.94 | 0.02020 |
| 40000 | 0.052 | 15.98 | 297.16 | 0.01869 |
| 40000 | 0.037 | 15.62 | 296.39 | 0.01361 |
| 40000 | 0.087 | 13.04 | 305.47 | 0.03300 |
| 40000 | 0.250 | 13.00 | 310.15 | 0.08970 |
| 50000 | 0.028 | 15.10 | 358.58 | 0.01025 |
| 50000 | 0.196 | 13.13 | 373.76 | 0.06872 |
| 50000 | 0.081 | 13.27 | 368.72 | 0.02956 |
| 50000 | 0.033 | 13.48 | 363.52 | 0.01258 |
| 50000 | 0.108 | 13.08 | 370.76 | 0.03914 |
| 50000 | 0.049 | 13.44 | 365.73 | 0.01848 |
| 50000 | 0.250 | 13.00 | 375.42 | 0.08704 |
| 60000 | 0.028 | 19.00 | 409.63 | 0.00913 |
| 60000 | 0.250 | 13.00 | 438.85 | 0.08496 |
| 60000 | 0.035 | 15.35 | 419.80 | 0.01235 |
| 60000 | 0.094 | 13.18 | 432.24 | 0.03359 |
| 60000 | 0.065 | 13.20 | 429.99 | 0.02377 |
| 60000 | 0.052 | 15.60 | 421.46 | 0.01777 |
| 60000 | 0.173 | 13.15 | 436.06 | 0.05968 |

*Rectangular channels*

The developing correlation results of the rectangular channels show that the formula optimized by the GA has a low accuracy for bend angles above 70°. Therefore, correlation constants were optimized for angles above 70°. After determining the constants of Eqs. 22 and 23 by the GA, the resulting correlations for *Nu* and *f* were obtained as follows:

$$Nu = 0.033Re^{0.839}\left(\frac{\alpha}{\pi}\right)^{0.071}\left(\frac{L_S}{X}\right)^{-0.023} \tag{36}$$

$$f = 0.41Re^{-0.204}\left(\frac{\alpha}{\pi}\right)^{0.323}\left(\frac{L_S}{X}\right)^{-0.043} \tag{37}$$

*Valid for* $10° \leq \alpha \leq 70°$

The mean relative errors for the predicted Nusselt number and friction factor in the rectangular channels were 2.75% and 6.11%, respectively.

Fig. 15 shows the Pareto curve for the rectangular channels, which includes a set of Pareto optimal points. Table 6 presents some optimal points based on the geometric parameters of the rectangular channel at different *Re*. Higher Nusselt numbers and lower friction factors were obtained at higher *Re*.

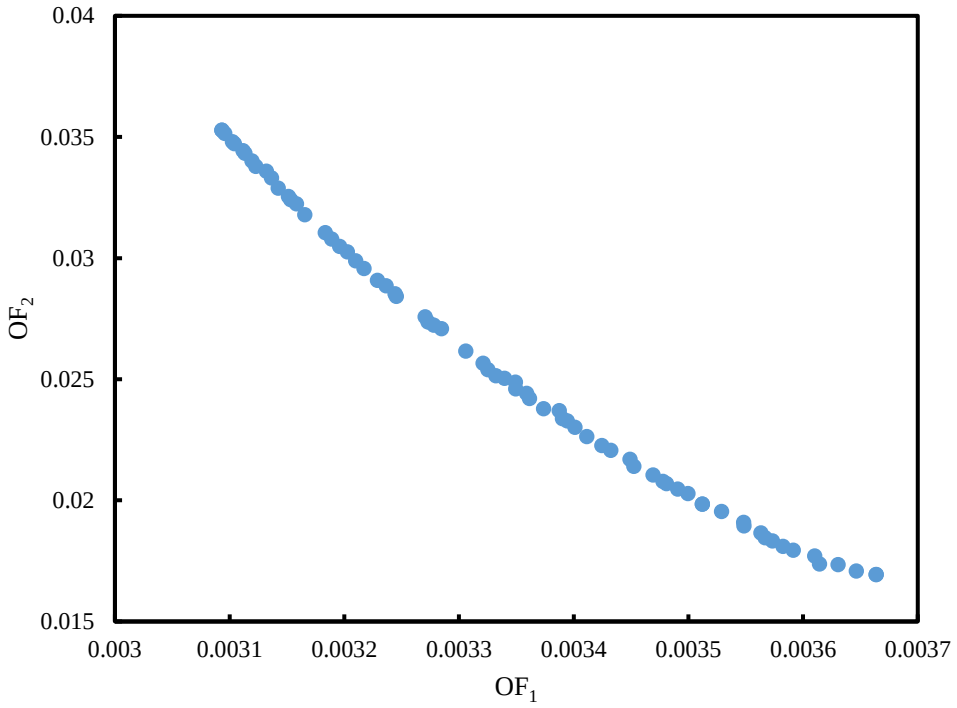


**Fig. 15**. Pareto optimal points for the rectangular channels

**Table 6**. Some optimal points selected for the rectangular channel.

| Re | α/π | $L_s$/X | Nu | f |
|---|---|---|---|---|
| 20000 | 0.0576 | 1.2999 | 108.76 | 0.02139 |
| 20000 | 0.5000 | 0.7000 | 128.61 | 0.04414 |
| 20000 | 0.1655 | 0.8407 | 118.40 | 0.03064 |
| 20000 | 0.1195 | 1.0555 | 115.09 | 0.02731 |
| 20000 | 0.3054 | 0.7232 | 124.09 | 0.03759 |
| 20000 | 0.0734 | 1.1025 | 111.06 | 0.02329 |
| 20000 | 0.2854 | 1.1785 | 122.12 | 0.03601 |
| 30000 | 0.0567 | 1.2637 | 152.75 | 0.01961 |
| 30000 | 0.1387 | 1.2384 | 162.84 | 0.02620 |
| 30000 | 0.3419 | 0.9062 | 174.87 | 0.03554 |
| 30000 | 0.4986 | 0.7118 | 180.62 | 0.04057 |
| 30000 | 0.1614 | 0.7565 | 166.48 | 0.02811 |
| 30000 | 0.2522 | 1.0576 | 170.52 | 0.03200 |
| 30000 | 0.0835 | 1.1830 | 157.24 | 0.02228 |
| 40000 | 0.4998 | 0.7580 | 229.63 | 0.03818 |
| 40000 | 0.0705 | 1.0401 | 198.36 | 0.02000 |
| 40000 | 0.2457 | 0.8426 | 217.81 | 0.03022 |
| 40000 | 0.1645 | 1.0458 | 210.64 | 0.02630 |
| 40000 | 0.1179 | 1.1481 | 205.28 | 0.02353 |
| 40000 | 0.0559 | 1.2803 | 194.19 | 0.01840 |
| 40000 | 0.3334 | 0.7871 | 222.93 | 0.03345 |
| 50000 | 0.0557 | 1.2876 | 234.10 | 0.01756 |
| 50000 | 0.4985 | 0.7002 | 277.36 | 0.03658 |
| 50000 | 0.0984 | 0.8941 | 245.79 | 0.02143 |
| 50000 | 0.1431 | 0.9406 | 252.13 | 0.02414 |
| 50000 | 0.3944 | 0.7582 | 272.29 | 0.03380 |
| 50000 | 0.0717 | 1.2874 | 238.33 | 0.01905 |
| 50000 | 0.2329 | 0.7903 | 262.04 | 0.02846 |
| 60000 | 0.0562 | 1.2688 | 273.03 | 0.01697 |
| 60000 | 0.2090 | 0.8591 | 302.43 | 0.02638 |
| 60000 | 0.0657 | 1.0416 | 277.35 | 0.01801 |
| 60000 | 0.1022 | 1.0388 | 286.21 | 0.02077 |
| 60000 | 0.4096 | 0.7143 | 318.58 | 0.03305 |
| 60000 | 0.4988 | 0.7133 | 323.08 | 0.03522 |

| | | | | |
|---|---|---|---|---|
| 60000 | 0.1465 | 0.8942 | 294.63 | 0.02348 |

*Serpentine channels*

Finally, the following correlations were proposed using GA for predicting *Nu* and *f* in the serpentine channels:

$$Nu = 0.035Re^{0.845}\left(\frac{L_S}{D_h}\right)^{-0.046}\left(\frac{R_C}{D_h}\right)^{-0.058} \quad (39)$$

$$f = 0.381Re^{-0.188}\left(\frac{L_S}{D_h}\right)^{-0.121}\left(\frac{R_C}{D_h}\right)^{-0.225} \quad (40)$$

The mean relative errors for *Nu* and *f* prediction in the investigated serpentine channels were 0.38% and 0.94%, respectively. Moreover, the optimal Pareto set is illustrated in Fig. 16. Some optimal points selected by multi-objective optimization are tabulated in Table 7.

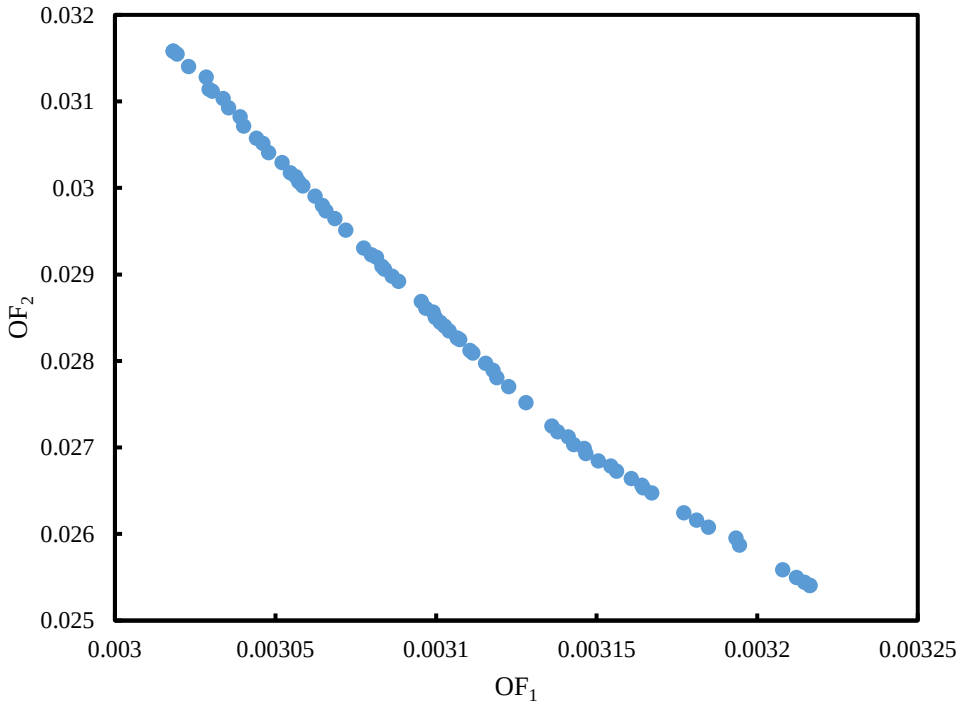


**Fig. 16**. Pareto optimal points in the serpentine channels

**Table 7**. Some optimal points selected for the serpentine channels

| Re | $L_s/D_h$ | $R_c/D_h$ | Nu | f |
|---|---|---|---|---|
| 20000 | 14.31 | 4.000 | 123.13 | 0.03141 |
| 20000 | 9.00 | 2.000 | 130.94 | 0.03883 |
| 20000 | 12.44 | 3.778 | 124.33 | 0.03236 |
| 20000 | 10.35 | 3.889 | 125.18 | 0.03287 |
| 20000 | 10.11 | 3.243 | 126.64 | 0.03434 |
| 20000 | 10.07 | 2.552 | 128.44 | 0.03626 |
| 20000 | 10.31 | 2.202 | 129.40 | 0.03738 |
| 30000 | 9.00 | 2.000 | 184.45 | 0.03598 |
| 30000 | 13.45 | 3.923 | 174.14 | 0.02945 |
| 30000 | 13.41 | 3.448 | 175.46 | 0.03033 |

| | | | | |
|---|---|---|---|---|
| 30000 | 14.76 | 2.846 | 176.65 | 0.03130 |
| 30000 | 9.42 | 2.235 | 182.88 | 0.03490 |
| 30000 | 9.02 | 2.896 | 180.52 | 0.03310 |
| 30000 | 15.00 | 4.000 | 173.07 | 0.02894 |
| 40000 | 14.99 | 4.000 | 220.70 | 0.02742 |
| 40000 | 12.33 | 3.419 | 224.73 | 0.02908 |
| 40000 | 10.68 | 2.237 | 231.86 | 0.03256 |
| 40000 | 9.00 | 2.000 | 235.21 | 0.03408 |
| 40000 | 10.14 | 3.338 | 227.08 | 0.02994 |
| 40000 | 9.89 | 2.764 | 229.84 | 0.03133 |
| 40000 | 9.50 | 2.216 | 233.23 | 0.03309 |
| 50000 | 13.18 | 3.054 | 272.31 | 0.02837 |
| 50000 | 10.13 | 2.588 | 278.28 | 0.03040 |
| 50000 | 14.95 | 3.997 | 266.54 | 0.02630 |
| 50000 | 9.16 | 2.118 | 282.85 | 0.03220 |
| 50000 | 9.00 | 2.000 | 284.02 | 0.03268 |
| 50000 | 11.37 | 2.779 | 275.67 | 0.02951 |
| 50000 | 14.34 | 3.640 | 268.51 | 0.02700 |
| 60000 | 14.98 | 3.995 | 310.92 | 0.02541 |
| 60000 | 9.00 | 2.000 | 331.32 | 0.03158 |
| 60000 | 12.38 | 3.308 | 317.10 | 0.02713 |
| 60000 | 9.43 | 2.385 | 327.26 | 0.03019 |
| 60000 | 9.86 | 3.175 | 321.21 | 0.02815 |
| 60000 | 9.38 | 2.786 | 324.40 | 0.02917 |
| 60000 | 12.83 | 3.993 | 313.15 | 0.02590 |

## Conclusion

In this study, the effects of geometric parameters on the thermal-hydraulic performance of zigzag, rectangular and serpentine channels were investigated using computational fluid dynamics. This technique makes it possible to extract data points in a wide range of geometrical parameters. The obtained Nusselt number and friction factor were higher than the straight channel in all channels. In the zigzag and rectangular channels, the *Nu* increased with increasing bend angles. In the serpentine channels, *Nu* decreased as the radius of the channel curvature increased.

On the other hand, the pressure drop in all channels increased with increasing the bend angles and radius of curvature of the channels. The highest *Nu* and *f* resulted for the zigzag channels. The *Nu* in this channel was 41% higher than the straight channel for the bend angle of 45°, $L_s$=13 cm in *Re*=60000. In addition, the *f* in this channel was increased by 465% compared to the straight channel in similar conditions. The genetic algorithm was used as a powerful technique to develop the predictive correlations for *Nu* and *f* in the investigated channels. The maximum prediction error (MRE) for the proposed correlations was 7.61%. The GA multi-objective optimization was used to select optimal geometrical dimensions of the studied heat exchangers. Designers can choose desired optimal geometry based on their preferences, such as thermal efficiency or pumping cost.

## Nomenclature

| | |
|---|---|
| $T$ | Temperature (K) |
| $S$ | Straight channel |
| $P$ | Pressure (Pa) |
| $A$ | Heat transfer area ($m^2$) |
| $OF$ | Objective function |
| $C_i$ | Constant |
| $L_{Path}$ | Length of path flow (m) |
| $L_S$ | Length of straight sections (m) |

| | |
|---|---|
| $L_c$ | Length of curvature sections(m) |
| $\Theta$ | The angle between two straight sections in the zigzag channel (°) |
| $\alpha$ | The angle between two straight sections in the rectangular channel (°) |
| $X$ | The length of a straight horizontal section in a rectangular channel(m) |
| $R_c$ | Radius of curvature (m) |
| $u$ | Velocity (m/s) |
| $Re$ | Reynolds number |
| $Nu$ | Nusselt number |
| $h$ | Convection heat transfer coefficient (W/m$^2$.K) |
| $\dot{Q}$ | Convection heat transfer rate (W/m$^2$.s) |
| $f$ | Friction factor |
| $\tau$ | Wall shear stress (Pa) |
| $\Delta P$ | Pressure drop (Pa) |
| $C_P$ | Specific heat (J/Kg.K) |
| $k$ | Thermal conductivity (W/m.K) |
| $D_h$ | Hydraulic diameter (m) |
| THP | Thermal-hydraulic performance |
| $P_k$ | Production of kinetic energy (kg/m.s$^3$) |

**Greek symbols**

| | |
|---|---|
| $\mu$ | Viscosity (Pa.s) |
| $\rho$ | Density (kg/m$^3$) |
| $\varepsilon$ | Turbulent dissipation rate (m$^2$/s$^3$) |

**Subscript**

| | |
|---|---|
| w | Wall |
| in | Inlet |
| out | Outlet |

## References


[1] Salimi S, Beigzadeh R. Computational fluid dynamics study and GA modeling approach of the bend angle effect on thermal-hydraulic characteristics in zigzag channels. Iranian Journal of Chemical Engineering (IJChE). 2019 Sep 1;16(3):70-83.

[2] Beigzadeh R, Parvareh A, Rahimi M. Experimental and CFD Study of the Tube Configuration Effect on the Shell-Side Thermal Performance in a Shell and Helically Coiled Tube Heat Exchanger. Iranian Journal of Chemical Engineering (IJChE). 2015 Apr 1;12(2):13-25.

[3] Ozbolat V, Tokgoz N, Sahin B. Flow characteristics and heat transfer enhancement in 2D corrugated channels. International Journal of Mechanical and Mechatronics Engineering. 2013 Sep 3;7(10):2074-8.

[4] Arvanitis KD, Bouris D, Papanicolaou E. Laminar flow and heat transfer in U-bends: The effect of secondary flows in ducts with partial and full curvature. International Journal of Thermal Sciences. 2018 Aug 1;130:70-93.

[5] Vickers NJ. Animal communication: when i'm calling you, will you answer too?. Current biology. 2017 Jul 24;27(14):R713-5.

[6] Lahimer AA, Alghoul MA, Sopian K, Khrit NG. Potential of solar reflective cover on regulating the car cabin conditions and fuel consumption. Applied thermal engineering. 2018 Oct 1;143:59-71.

[7] Shi H, Raimondi ND, Fletcher DF, Cabassud M, Gourdon C. Numerical study of heat transfer in square millimetric zigzag channels in the laminar flow regime. Chemical Engineering and

Processing-Process Intensification. 2019 Oct 1;144:107624.

[8] Chen M, Sun X, Christensen RN. Thermal-hydraulic performance of printed circuit heat exchangers with zigzag flow channels. International Journal of Heat and Mass Transfer. 2019 Mar 1;130:356-67.

[9] Vickers NJ. Animal communication: when i'm calling you, will you answer too?. Current biology. 2017 Jul 24;27(14):R713-5.

[10] Thippavathini S, Das AK. Passage of a Liquid Taylor Drop through Successive Bends in a Rectangular Channel. Industrial & Engineering Chemistry Research. 2020 Oct 9;59(42):19045-61.

[11] Spizzichino M, Sinibaldi G, Romano GP. Experimental investigation on fluid mechanics of micro-channel heat transfer devices. Experimental Thermal and Fluid Science. 2020 Oct 1;118:110141.

[12] Yan WT, Li C, Ye WB. Numerical investigation of hydrodynamic and heat transfer performances of nanofluids in a fractal microchannel heat sink. Heat Transfer—Asian Research. 2019 Sep;48(6):2329-49.

[13] Mitra P, Dutta S, Hens A. Separation of particles in spiral micro-channel using Dean's flow fractionation. Journal of the Brazilian Society of Mechanical Sciences and Engineering. 2020 Aug;42(8):1-2.

[14] Hassanzadeh R, Abadtalab M, Bayat A. Optimization of Wave Inclination Angle in Parallel Wavy-Channel Heat Exchangers. Arabian Journal for Science and Engineering. 2020 Feb;45(2):817-32.

[15] Abbasi FM, Shehzad SA. Impact of Curvature-Dependent Channel Walls on Peristaltic Flow of Newtonian Fluid Through a Curved Channel with Heat Transfer. Arabian Journal for Science and Engineering. 2020 Nov;45:9037-44.

[16] Morini GL. Single-phase convective heat transfer in microchannels: a review of experimental results. International journal of thermal sciences. 2004 Jul 1;43(7):631-51.

[17] Loew RM. Determinants of divorced older women's labor supply. Research on Aging. 1995 Dec;17(4):385-411.

[18] Zhou J, Ke H, Deng X. Experimental and CFD investigation on temperature distribution of a serpentine tube type photovoltaic/thermal collector. Solar Energy. 2018 Nov 1;174:735-42.

[19] Wang M, Zhu W. Pore-scale study of heterogeneous chemical reaction for ablation of carbon fibers using the lattice Boltzmann method. International Journal of Heat and Mass Transfer. 2018 Nov 1;126:1222-39.

[20] Plouffe P, Roberge DM, Sieber J, Bittel M, Macchi A. Liquid–liquid mass transfer in a serpentine micro-reactor using various solvents. Chemical Engineering Journal. 2016 Feb 1;285:605-15.

[21] Dewan A, Mahanta P, Raju KS, Kumar PS. Review of passive heat transfer augmentation techniques. Proceedings of the Institution of Mechanical Engineers, Part A: Journal of Power and Energy. 2004 Nov 1;218(7):509-27.

[22] Elshafei EA, Mohamed MS, Mansour H, Sakr M. Experimental study of heat transfer in pulsating turbulent flow in a pipe. International Journal of Heat and Fluid Flow. 2008 Aug 1;29(4):1029-38.

[23] Bharadwaj P, Khondge AD, Date AW. Heat transfer and pressure drop in a spirally grooved tube with twisted tape insert. International Journal of Heat and Mass Transfer. 2009 Mar 1;52(7-8):1938-44.

[24] Imran AA, Mahmoud NS, Jaffal HM. Numerical and experimental investigation of heat transfer in liquid cooling serpentine mini-channel heat sink with different new configuration models. Thermal Science and Engineering Progress. 2018 Jun 1;6:128-39.

[25] Omidi M, Farhadi M, Darzi AA. Numerical study of heat transfer on using lobed cross sections in helical coil heat exchangers: effect of physical and geometrical parameters. Energy conversion and management. 2018 Nov 15;176:236-45.

[26] De la Torre R, Francois JL, Lin CX. Optimization and heat transfer correlations development of zigzag channel printed circuit heat exchangers with helium fluids at high temperature. International Journal of Thermal Sciences. 2021 Feb 1;160:106645.

[27] Donaldson AA, Kirpalani DM, Macchi A. Single and two-phase pressure drop in serpentine mini-channels. Chemical Engineering and Processing: Process Intensification. 2011 Aug 1;50(8):877-84.

[28] Korpyś M, Dzido G, Al-Rashed MH, Wójcik J. Experimental and numerical study on heat transfer intensification in turbulent flow of CuO–water nanofluids in horizontal coil. Chemical Engineering and Processing-Process Intensification. 2020 Jul 1;153:107983.
[29] Beigzadeh R, Eiamsa-ard S. Genetic algorithm multiobjective optimization of a thermal system with three heat transfer enhancement characteristics. Journal of Enhanced Heat Transfer. 2020;27(2).
[30] Yang Y, Li H, Yao M, Zhang Y, Zhang C, Zhang L, Wu S. Optimizing the size of a printed circuit heat exchanger by multi-objective genetic algorithm. Applied Thermal Engineering. 2020 Feb 25;167:114811.
[31] Yıldızeli A, Çadırcı S. Multi objective optimization of a micro-channel heat sink through genetic algorithm.
[32] Beigzadeh R, Rahimi M, Parvizi M. Experimental study and genetic algorithm-based multi-objective optimization of thermal and flow characteristics in helically coiled tubes. Heat and Mass Transfer. 2013 Sep;49(9):1307-18.
[33] Rahimi M, Shabanian SR, Alsairafi AA. Experimental and CFD studies on heat transfer and friction factor characteristics of a tube equipped with modified twisted tape inserts. Chemical Engineering and Processing: Process Intensification. 2009 Mar 1;48(3):762-70.
[34] Taler D, Taler J. Simple heat transfer correlations for turbulent tube flow. InE3S Web of conferences 2017 (Vol. 13, p. 02008). EDP Sciences.
[35] Konak A, Coit DW, Smith AE. Multi-objective optimization using genetic algorithms: A tutorial. Reliability engineering & system safety. 2006 Sep 1;91(9):992-1007.

**How to cite**: *Saeid Salimi, Reza Beigzadeh. Multi-Objective Optimization of Different Channel Shapes in heat Heat Exchangers. Journal of Chemical and Petroleum Engineering*. 2021; 55(2): 293-318.